Applied Clay Science 46 (2009) 21–26

Contents lists available at ScienceDirect

Applied Clay Science

journal homepage: www.elsevier.com/locate/clay

Preparation and swelling properties of superabsorbent nanocomposites based on natural guar gum and organo-vermiculite

Wenbo Wang [a,b], Junping Zhang [a], Aiqin Wang [a,*]

[a] Center for Eco-material and Green Chemistry, Lanzhou Institute of Chemical Physics, Chinese Academy of Sciences, Lanzhou, 730000, PR China
[b] Graduate School of the Chinese Academy of Sciences, Beijing, 100049, PR China

ARTICLE INFO

Article history:
Received 22 February 2009
Received in revised form 28 June 2009
Accepted 2 July 2009
Available online 3 August 2009

Keywords:
Guar gum
Organo-vermiculite
Superabsorbent
Swelling
Graft copolymerization
Nanocomposites

ABSTRACT

Vermiculite (VMT) was modified with cetyl trimethylammonium bromide (CTAB). Superabsorbent nanocomposites were prepared by solution polymerization of natural guar gum (GG), partially neutralized acrylic acid (NaA) and organo-vermiculite (CTA^+-VMT), ammonium persulfate (APS) as initiator and *N*,*N*′-methylene-bis-acrylamide (MBA) as crosslinking agent. FTIR spectra confirmed that NaA had been grafted onto GG and the –OH groups of CTA^+-VMT participated in the polymerization reaction. The intercalated-VMT was exfoliated during polymerization and uniformly dispersed in the GG-*g*-PNaA matrix. Swelling tests show that CTA^+-VMT improved swelling and swelling rate more remarkably than VMT, and the nanocomposite exhibited distinct kinetic swelling behavior in NaCl and $CaCl_2$ solution. Organo-VMT improved the gel strength of the nanocomposite compared to VMT, and the maximum storage modulus of the nanocomposite reached 658 Pa ($\gamma = 0.5\%$, $\omega = 100$ rad/s).

1. Introduction

Composite of polymers with clay minerals has long been an interesting subject of scientific research and industrial applications because the incorporation of clay minerals can reduce production cost and improve the performance of material (Ray and Okamoto, 2003; Liu, 2007; Bergaya et al., 2006a). Superabsorbents are hydrophilic polymer networks which can absorb and retain large amounts of aqueous fluids. Superabsorbents have found extensive applications in many fields such as agriculture (Puoci et al., 2008; Chu et al., 2006), hygienic products (Kamat and Malkani, 2003; Kosemund et al., 2008), wastewater treatment (Wang et al., 2008; Kaşgöz et al., 2008) and drug-delivery systems (Sadeghi and Hosseinzadeh, 2008; Omidian et al., 2005), etc. However, the conventional superabsorbents are based on expensive fully petroleum-based polymers, their production consumes lots of petroleum and their usage can also cause a non-negligible environment problem (Kiatkamjornwong et al., 2002). New types of superabsorbents by introducing naturally available raw materials as additives were desired. Because of the low cost, easy availability and environmentally friendly characteristic, clay minerals exhibit superiority to other materials for designing superabsorbent materials.

Recently, due to the increasing public attention to environment topics, polysaccharide-based materials have attracted much interest (Pourjavadi et al., 2006; Wu et al., 2003) and the organo-inorganic superabsorbent nanocomposites based on natural polysaccharides and clay minerals undoubtedly become desired materials because they have both excellent performance and environmental friendly characteristics (Ray and Bousmina, 2005). However, owing to the extreme viscosity of natural polysaccharide, the particles of clay minerals are hardly dispersed uniformly in the matrix during polymerization, and the resultant materials also fail to exhibit optimal performance. For this reason, the clay minerals have to be modified before compounding (Pavlidou and Papaspyrides, 2008; Lee and Chen, 2005). A popular and relatively easy method for modifying clay minerals, making them more compatible with an organic matrix, is intercalating cationic surfactants (de Paiva et al., 2008; Zhu et al., 2008; Bergaya et al., 2006b), the modified clay mineral showed improved dispersion in polymeric matrix (Huang et al., 2009).

The properties of traditional superabsorbent could be enhanced by incorporating VMT (Zheng et al., 2007). It is expected that organo-modification of VMT can further improve dispersion and performance of the resultant nanocomposite.

Guar gum (GG) derived from the seeds of guar plant *Cyanaposis tetragonolobus* (Leguminosae) is a natural nonionic branched polymer with β-D-mannopyranosyl units linked (1–4) with single membered α-D-galactopyranosyl units occurring as side branches (Scheme 1). GG and its derivatives have been used in various fields (e.g. thickening agent, ion exchange resin and dispersing agent, etc.).

A series of guar gum-*g*-poly(sodium acrylate)/organo-vermiculite (GG-*g*-PNaA/CTA^+-VMT) nanocomposites was prepared and

* Corresponding author. Tel.: +86 931 4968118; fax: +86 931 8277088.
E-mail address: aqwang@lzb.ac.cn (A. Wang).

0169-1317/$ – see front matter © 2009 Elsevier B.V. All rights reserved.
doi:10.1016/j.clay.2009.07.001

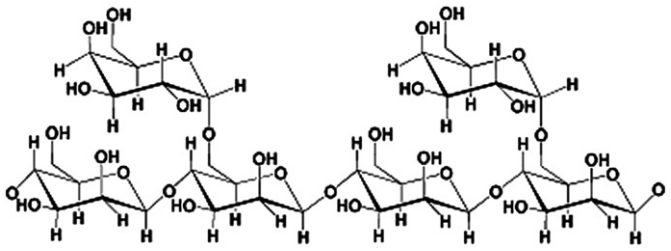

Scheme 1. Structure of natural guar gum.

characterized by Fourier transform infrared spectroscopy (FTIR), X-ray diffraction (XRD) and transmission electron microscopy (TEM). The swelling behavior and gel strength were also determined.

2. Experimental

2.1. Materials

Guar gum (GG, food grade, number average molecular weight 220,000) was from Wuhan Tianyuan Biology Co., China. Acrylic acid (AA, chemically pure, Shanghai Shanpu Chemical Factory, Shanghai, China) was distilled under reduced pressure before use. Ammonium persulfate (APS, analytical grade, Xi'an Chemical Reagent Factory, China), *N*,*N*′-methylene-bis-acrylamide (MBA, chemically pure, Shanghai Chemical Reagent Corp., China) and cetyl trimethylammonium bromide (CTAB, Beijing Chemical Reagents Company, China) were used as received. Unexpanded vermiculite (VMT) micropowder (Linze Colloidal Co., Gansu, China) was milled and passed through a 320-mesh screen before use. The other reagents used were of analytical grade and all solutions were prepared with distilled water.

2.2. Preparation of organo-VMT

A series of organo-VMT (CTA^+-VMT) samples with various CTA contents was prepared as follows. Five different amounts of CTAB were dissolved in 100 mL distilled water, respectively, and then 10.0 g of VMT was suspended in the solution by vigorous stirring (1200 r/min) for 4 h at room temperature. CTA^+-VMT was separated by filtration and washed with a large volume of distilled water to remove excess CTAB until in the filtrate no Br^- was detected by 0.1 M $AgNO_3$ solution. CTA^+-VMT was dried to constant mass at 70 °C and passed through a 320-mesh sieve (46 μm).

The CTA content (denoting the mass percent of organic cation in CTA^+-VMT sample) was determined by thermogravimetry. 0.5 g of CTA^+-VMT and raw VMT was calcined in a muffle furnace in air at 800 °C for 6 h. After reaching a constant mass, the samples were transferred into a desiccator and cooled to room temperature. These samples were weighed and the CTA content was derived from the mass loss related to the mass loss of unmodified vermiculite (Table 1).

2.3. Preparation of GG-g-PNaA/CTA^+-VMT

GG (1.20 g) was dispersed in 34 mL of 0.067 M NaOH solution (pH 12.5) in a 250 mL four-necked flask equipped with a mechanical stirrer, a reflux condenser, a thermometer and a nitrogen line, and the dispersions were heated in an oil bath to 60 °C and kept for 1 h to form a colloidal slurry. Then, 4 mL of the aqueous solution of the initiator APS (0.1008 g) was added to the reaction flask under continuous stirring and kept at 60 °C for 10 min. 7.2 g of acrylic acid was neutralized using 8.5 mL of 8 M NaOH to reach a total neutralization degree of 70% (under consideration of the 34 mL of 0.067 M NaOH solution used to disperse GG), and then crosslinker MBA (21.6 mg) and CTA^+-VMT powder (0.45 g) were charged into the neutralized acrylic acid solution under magnetic stirring. After cooling to 40 °C, the dispersion was added into the reaction flask, and temperature was slowly risen to 70 °C and kept for 3 h to complete polymerization. A nitrogen atmosphere was maintained throughout the reaction period. The obtained gel products were dried to a constant mass at 70 °C and ground and passed through 40–80-mesh sieve (180–380 μm).

Table 1
CTAB addition and the resultant CTA content.

Mass of CTAB (g)	Mass of VMT (g)	Volume of dispersion (mL)	CTA content (mass%)
0.3132	10	100	2.06
0.6263	10	100	2.62
1.2526	10	100	4.03
2.5052	10	100	9.01
3.7578	10	100	12.16

2.4. Measurements of equilibrium water absorption and swelling kinetics

0.05 g of dry samples was immersed in excess aqueous solutions at room temperature for 4 h to reach swelling equilibrium. The swollen gels were filtered using a mesh sieve, and then drained on the sieve for 10 min until no free water remained. After weighing the swollen samples, the equilibrium water absorption was derived from the mass changes.

Swelling kinetics of superabsorbent in aqueous solutions was measured as follows: 0.05-g samples were contacted with 200 mL solution. The swollen gels were filtered by a sieve after different time periods, and the water absorption was derived from the mass changes. In all cases three parallel samples were used and the average values were reported in this paper.

2.5. Characterizations

FTIR spectra were recorded on a Nicolet NEXUS FTIR spectrometer in 4000–400 cm^{-1} region using KBr platelets. XRD analyses were performed using an X-ray power diffractometer with Cu anode (PAN analytical Co. X'pert PRO), running at 40 kV and 30 mA, scanning from 3° to 10° at 3°/min. TEM was performed on an instrument of JEM1200EX (Japan), and the powdered specimen was placed on the copper grids after sonicating its suspension in ethanol dried for 30 min. The gel strength of the swollen composites was determined with the Physica MCR 301 rheometer (Germany) at 25 °C according to a previously developed method (Ramazani-Harandi et al., 2006). The tested samples were swollen in 0.9 mass% NaCl solution. The strain amplitude was chosen as 0.5% and the angular frequency ω was defined in the range of 0.1–100 rad/s. The results were the average values of at least 3 measurements.

3. Results and discussion

3.1. FTIR spectra

The FTIR spectra of CTA^+-VMT showed strong absorption bands at 2914 and 2848 cm^{-1} (asymmetrical stretching vibration and symmetrical stretching vibration of $-CH_3$ and $-CH_2$, respectively), and the medium bands at 1486 and 1466 cm^{-1} (bending vibration of C–H) (Fig. 1). The intensity of above bands increased with increasing CTA content.

The spectra in Fig. 1(g–i) are noticed in the weakened absorption bands of GG at 1017, 1082 and 1158 cm^{-1} (stretching vibrations of C–OH) and the band at 1648 cm^{-1} (bending vibration of –OH groups) and new bands at 1563 cm^{-1} for GG-*g*-PNaA, 1569 cm^{-1} for GG-*g*-PNaA/CTA^+-VMT, 1457 and 1403 cm^{-1} (asymmetric stretching and symmetric stretching in $-COO^-$ groups, respectively). This observation reveals that NaA had been grafted onto GG backbone. The –OH stretching vibration of VMT at 3668 and 3442 cm^{-1} and the

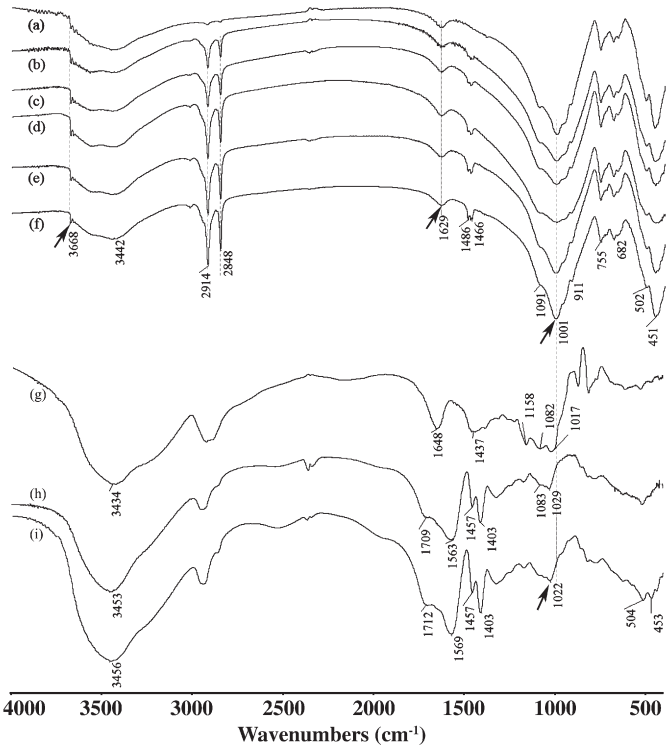

Fig. 1. FTIR spectra of VMT (a), CTA^+-VMT with CTA content of (b) 2.06 mass%, (c) 2.62 mass%, (d) 4.03 mass%, (e) 9.01 mass% and (f) 12.16 mass%, (g) GG, (h) GG-*g*-PNaA and (i) GG-*g*-PNaA/CTA^+-VMT (CTA content, 4.03 mass%; CTA^+-VMT content, 5 mass%).

–OH bending vibration of VMT at 1629 cm^{-1} almost disappeared after reaction (Fig. 1(h, i)). The absorption band of VMT at 1001 cm^{-1} attributed to ≡Si–O stretching shifted to 1022 cm^{-1} in the spectrum of GG-*g*-PNaA/VMT. These informations indicate that VMT also participated in the graft copolymerization reaction through silanol groups (Li et al., 2004).

3.2. XRD analysis

VMT showed a strong (001) reflection at $2\theta = 7.17°$ with a basal spacing (d) of 1.23 nm (Fig. 2a). This reflection shifted to $2\theta = 4.61°$ ($d = 1.92$ nm), 5.06° ($d = 1.75$ nm), 6.86° ($d = 1.29$ nm) after modification with CTA^+ (Fig. 2b), indicating that the CTA^+ cations were intercalated. However, no VMT reflections could be observed in the XRD patterns of the nanocomposites even if the content of CTA^+-VMT reached 20 mass% (Fig. 2(c, d)). Thus, CTA^+-VMT was almost exfoliated and the VMT platelets were thoroughly dispersed in the polymer matrix (Liu et al., 2007; Al et al., 2008). A similar observation was made for superabsorbent nanocomposites based on starch grafted PAA-*co*-AM/MMT (Luo et al., 2005).

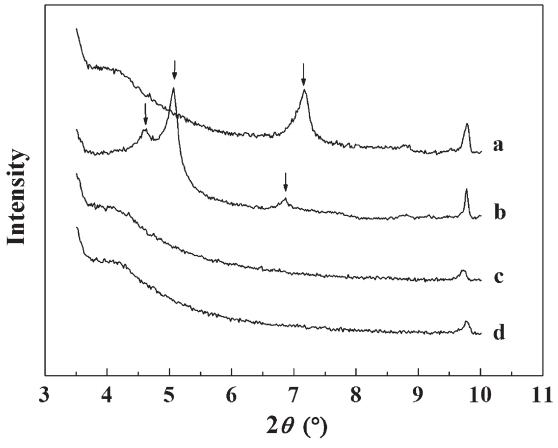

Fig. 2. XRD patterns of (a) natural VMT, (b) CTA^+-VMT (CTA content, 4.03 mass%), (c) GG-*g*-PNaA/CTA^+-VMT (CTA content, 4.03 mass%; CTA^+-VMT content, 5 mass%) and (d) GG-*g*-PNaA/CTA^+-VMT (CTA content, 4.03 mass%; CTA^+-VMT content, 20 mass%).

3.3. TEM analysis

TEM analysis (Fig. 3) revealed the good dispersion of CTA^+-VMT in GG-*g*-PNaA/CTA^+-VMT (CTA content, 4.03 mass%; CTA^+-VMT content, 5 mass%). Due to the expansion of the interlayer space by intercalation of CTA^+, the vermiculite particles exfoliated during the polymerization reaction.

3.4. Effects of CTA content on water absorption

The CTA content of the modified vermiculite had a great influence on water absorption of the nanocomposites (Fig. 4). The water absorption of the nanocomposite containing 5 mass% CTA^+-VMT was always higher than that of GG-*g*-PNaA/VMT. Water absorption was highest (575 $g \cdot g^{-1}$) at a CTA content of 4.03 mass%. At the surface of CTA^+-VTM particles, the hydrogen bond interaction between hydrophilic polymeric chains with –COOH and $-COO^-$ groups can be weakened and tangling of polymer chains was restricted. Secondly, the long alkyl chains can act as obstructers for the radical polymerization reaction, the opportunity for cyclization reaction of MBA increases and the network becomes reasonably crosslinked and therefore swells to a higher degree (Elliott et al., 2004). The exfoliation of the CTA^+-VMT particles will also improve water absorption.

With increasing the CTA content beyond 4.03 mass%, the increased number of alkyl chains reduced the polymerization efficiency and the hydrophility of the polymer material. Consequently, water absorption was reduced.

3.5. Effects of CTA^+-VMT content on water absorption

The water absorption of the nanocomposites with increasing CTA^+-VMT content showed a maximum at 5 mass% (Fig. 5). The incorporation of rigid VMT particles prevented intertwining of grafted polymeric chains and weakens the hydrogen-bonding interaction between –COOH groups. This decreased the degree of physical crosslinking and improved water absorption.

According to literature (Lin et al., 2001), ultrafine clay mineral powder may act as additional crosslinking points in polymer networks. Thus, the addition of VMT may increase the crosslinking

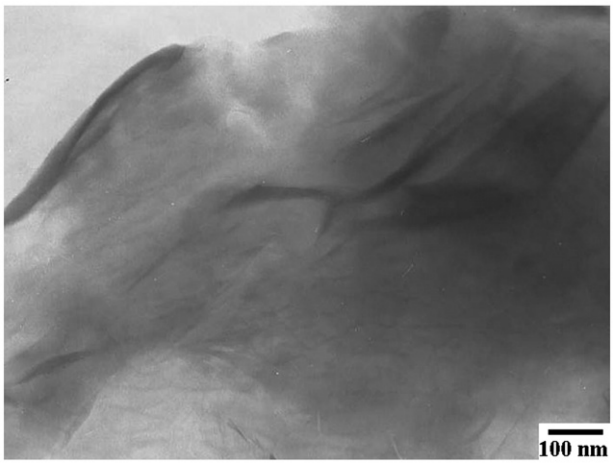

Fig. 3. TEM micrographs of superabsorbent nanocomposite GG-*g*-PNaA/CTA^+-VMT (CTA content, 4.03 mass%; CTA^+-VMT content, 5 mass%).

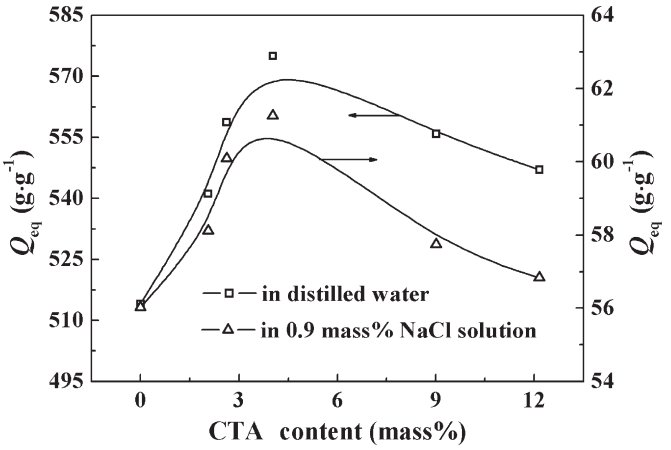

Fig. 4. Variation of equilibrium water absorption for the GG-*g*-PNaA/CTA$^+$-VMT (5 mass%) superabsorbent nanocomposite with different CTA contents.

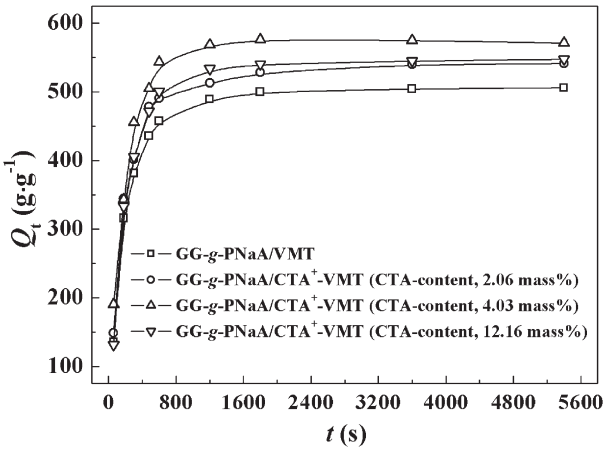

Fig. 6. Swelling kinetic curves of GG-*g*-PNaA/CTA$^+$-VMT (5 mass%) with various CTA contents in distilled water.

density of the nanocomposite and minimize the network voids for holding water. In addition, the excess VMT may fill the voids, decreasing the hydrophilicity of the nanocomposite. As a result, water absorption decreased with increase of the VMT content above 5 mass%. A similar tendency was observed for poly(sodium acrylate)/vermiculite superabsorbent (Zheng et al., 2007).

3.6. Effect of CTA content on swelling rate in distilled water

Fig. 6 represents swelling of the nanocomposites of 180–380 μm in distilled water as a function of time. The swelling rate of the nanocomposites increased steeply within 1200 s, then reached a plateau. The swelling kinetics can be expressed by the Voigt viscoelastic model (Eq. (1)) (Omidian et al., 1998; Kabiri et al., 2003).

$$Q_t = Q_\infty\left(1 - e^{-t/r}\right) \quad (1)$$

where Q_t (g•g^{-1}) is swelling at time t, Q_∞ (g•g^{-1}) is the power parameter (g•g^{-1}), denoting the theoretical equilibrium water absorption; t (s) is swelling time, and r (s) stands for a rate parameter, denoting the time required to reach 63% of equilibrium water absorption. The values of r and Q_∞ were calculated by fitting the experimental data by Eq. (1) (Table 2). Because r is a measure of resistance to water permeation, lower r values reflect higher swelling rates (Pourjavadi and Mahdavinia, 2006). Thus, the swelling rate decreased in the order: GG-*g*-PNaA/CTA$^+$-VMT (CTA content, 4.03 mass%) > GG-*g*-PNaA/CTA$^+$-VMT (CTA content, 2.06 mass%) > GG-*g*-PNaA/CTA$^+$-VMT (CTA content, 12.16 mass%) > GG-*g*-PNaA/VMT. Obviously, moderate organification (CTA content <4.03 mass%) of VMT improved the swelling whereas higher CTA contents decreased it. As is discussed above, moderate CTA contents may improve the three-dimensional network structure of the superabsorbent due to the formation of small hydrophobic region in the polymer matrix. The improvement of network structure is favorable to the diffusion of water molecules into the network and to the relaxation of polymer chains. Therefore, moderate CTA contents help to increase the swelling rate. Higher CTA contents will increase the amounts of long alkyl chains in polymer network and decrease the hydrophilicity of polymer. This restricts the rapid diffusion of water molecules and reduced the swelling rate.

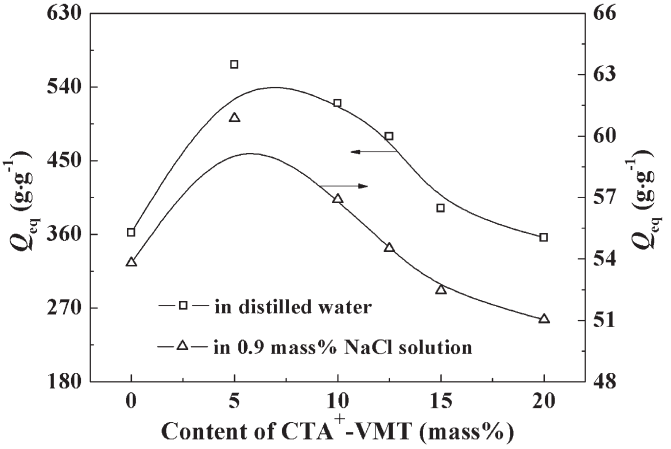

Fig. 5. Effects of the content of CTA$^+$-VMT (CTA content, 4.03 mass%) on the water absorption.

3.7. Swelling in saline solution

Water absorption of the nanocomposite increased with prolonged contact time and reached a swelling equilibrium within 1200 s in NaCl solution. In $CaCl_2$ solution, the water absorption increased to 117 g•g^{-1} during the first 600 s, and then decreased until swelling almost disappeared (Fig. 7). This successive swelling–deswelling process is known as overshooting effect (Díez-Peña et al., 2003), and may be ascribed to the additional crosslinking action of Ca^{2+} ions due to the interaction with the $-COO^-$ groups of the polymer chains. FTIR spectra (Fig. 8) showed the change of chemical environment of $-COO^-$ groups of GG-*g*-PNaA/CTA$^+$-VMT after swelling in NaCl and $CaCl_2$ solution. The absorption band of $-COO^-$ groups did not change after swelling in 5 mM NaCl solution, but shifted to 1546 cm^{-1} after swelling in 5 mM $CaCl_2$ solution.

3.8. Gel strength

The storage modulus (G') of the nanocomposites GG-*g*-PNaA/CTA$^+$-VMT (CTA content = 2.06, 2.62, 4.03, 9.01 mass%) was higher than that of GG-*g*-PNaA/VMT (Fig. 9), indicating that the moderate organification of VMT is favorable to enhance the gel strength of the

Table 2
Swelling kinetics of the superabsorbents containing 5 mass% of VMT.

Sample	Q_∞ (g·g^{-1})	r (s)
GG-*g*-PNaA/VMT	495	195.51
GG-*g*-PNaA/CTA$^+$-VMT (CTA content, 2.06 mass%)	526	188.73
GG-*g*-PNaA/CTA$^+$-VMT (CTA content, 4.03 mass%)	569	185.80
GG-*g*-PNaA/CTA$^+$-VMT (CTA content, 12.16 mass%)	534	204.31

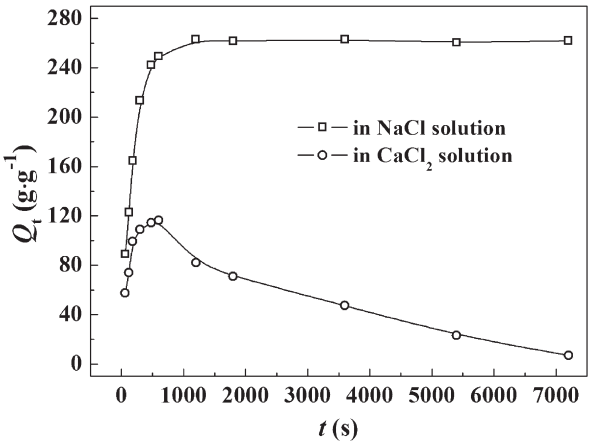

Fig. 7. Kinetic swelling curves of GG-*g*-PNaA/CTA$^+$-VMT (CTA content, 4.03 mass%; CTA$^+$-VMT content, 5 mass%) in 5 mM NaCl and $CaCl_2$ solutions.

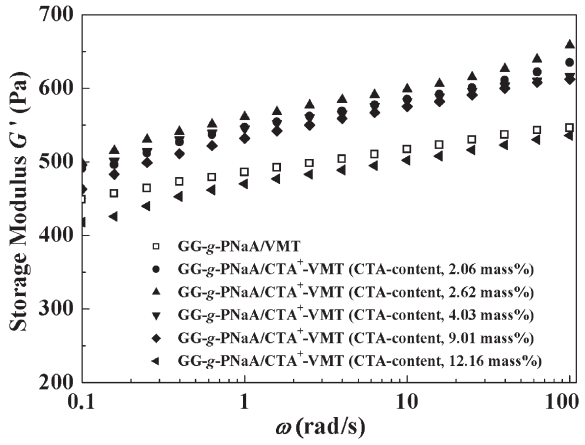

Fig. 9. Angular frequency (ω) dependence of the storage modulus (G') at a constant strain (0.5%) for the nanocomposites swollen in 0.9 mass% NaCl solution.

nanocomposite. G' was reduced when the CTA content exceeded 12.16 mass%. This may be attributed to polymerization inhibition by the long hydrophobic alkyl chains of CTA$^+$-VMT during polymerization, which affected the crosslinking and cyclization reaction of crosslinker (Elliott et al., 2004). GG-*g*-PNaA/CTA$^+$-VMT with the CTA content of 2.62 mass% showed the maximum G' of 498 Pa ($\gamma = 0.5\%$, $\omega = 0.1$ rad/s) and 658 Pa ($\gamma = 0.5\%$, $\omega = 100$ rad/s).

4. Conclusions

As a part of the efforts to reduce the excessive consumption of petroleum resources and the environmental impact resulting from industrial polymers, superabsorbent nanocomposites were prepared from natural guar gum and organo-vermiculite by solution polymerization. FTIR, XRD and TEM analyses indicated that CTA$^+$-VMT was exfoliated during polymerization and uniformly dispersed in the GG-*g*-PNaA matrix. The exfoliated platelets participated in the polymerization reaction through −OH groups. GG-*g*-PNaA/CTA$^+$-VMT led to better dispersion of VMT platelets. CTA$^+$-VMT enhanced the water absorption and swelling rate. The swelling rate of GG-*g*-PNaA/CTA$^+$-VMT had a maximum at CTA content of 4.03 mass%. The gel strength of the swollen GG-*g*-PNaA/CTA$^+$-VMT nanocomposites was improved compared to that of GG-*g*-PNaA/VMT, the maximum storage modulus reached 658 Pa ($\gamma = 0.5\%$, $\omega = 100$ rad/s). Thus, superabsorbent nanocomposites based on renewable and biodegradable natural GG and modified vermiculite exhibited satisfactory swelling capability and swelling rate, which can be used as potential water-manageable materials for various applications.

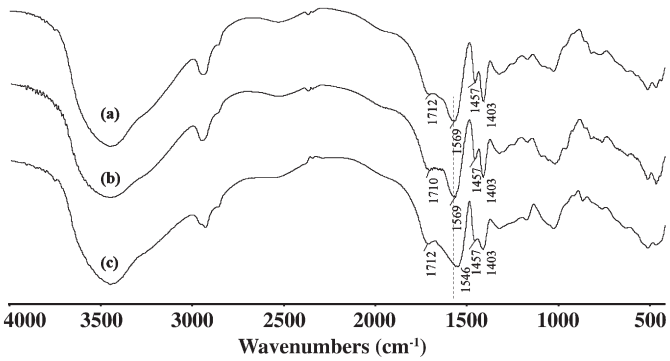

Fig. 8. FTIR spectra of (a) GG-*g*-PNaA/CTA$^+$-VMT (CTA content, 4.03 mass%; CTA$^+$-VMT content, 5 mass%) nanocomposite, (b) the nanocomposite after swelling in 5 mM NaCl solution and (c) the nanocomposite after swelling in 5 mM $CaCl_2$ solution.

Acknowledgements

This work was financially supported by the Western Action Project of CAS (no. KGCX2-YW-501) and "863" Project of the Ministry of Science and Technology, P. R. China (no. 2006AA03Z0454 and 2006AA100215).

References

Al, E., Güçlü, G., İyim, T.B., Emik, S., Özgümüş, S., 2008. Synthesis and properties of starch-*graft*-acrylic acid/Na-montmorillonite superabsorbent nanocomposite hydrogels. J. Appl. Polym. Sci. 109, 16–22.

Bergaya, F., Theng, B.K.G., Lagaly, G. (Eds.), 2006a. Handbook of Clay Science. Developments in Clay Science, vol. 1. Elsevier, Amsterdam, pp. 583–621. Chapter 10.3.

Bergaya, F., Theng, B.K.G., Lagaly, G. (Eds.), 2006b. Handbook of Clay Science. Developments in Clay Science, vol. 1. Elsevier, Amsterdam. Chapter 7.3.

Chu, M., Zhu, S.Q., Li, H.M., Huang, Z.B., Li, S.Q., 2006. Synthesis of poly(acrylic acid)/sodium humate superabsorbent composite for agricultural use. J. Appl. Polym. Sci. 102, 5137–5143.

de Paiva, L.B., Morales, A.R., Valenzuela Díaz, F.R., 2008. Organoclays: properties, preparation and applications. Appl. Clay Sci. 42, 8–24.

Díez-Peña, E., Quijada-Garrido, I., Barrales-Rienda, J.M., 2003. Analysis of the swelling dynamics of cross-linked P(N-iPAAm-*co*-MAA) copolymers and their homopolymers under acidic medium. A kinetics interpretation of the overshooting effect. Macromolecules 36, 2475–2483.

Elliott, J.E., Macdonald, M., Nie, J., Bowman, C.N., 2004. Structure and swelling of poly (acrylic acid) hydrogels: effect of pH, ionic strength, and dilution on the crosslinked polymer structure. Polymer 45, 1503–1510.

Huang, X.J., Xu, S.M., Zhong, M., Wang, J.D., Feng, S., Shi, R.F., 2009. Modification of Na-bentonite by polycations for fabrication of amphoteric semi-IPN nanocomposite hydrogels. Appl. Clay Sci. 42, 455–459.

Kabiri, K., Omidian, H., Hashemi, S.A., Zohuriaan-Mehr, M.J., 2003. Synthesis of fast-swelling superabsorbent hydrogels: effect of crosslinker type and concentration on porosity and absorption rate. Eur. Polym. J. 39, 1341–1348.

Kamat, M., Malkani, R., 2003. Disposable diapers: a hygienic alternative. Indian J. Pediatr. 70, 879–881.

Kaşgöz, H., Durmus, A., Kaşgöz, A., 2008. Enhanced swelling and adsorption properties of AAm-AMPSNa/clay hydrogel nanocomposites for heavy metal ion removal. Polym. Adv. Technol. 19, 213–220.

Kiatkamjornwong, S., Mongkolsawat, K., Sonsuk, M., 2002. Synthesis and property characterization of cassava starch grafted poly[acrylamide-*co*-(maleic acid)] superabsorbent via γ-irradiation. Polymer 43, 3915–3924.

Kosemund, K., Schlatter, H., Ochsenhirt, J.L., Krause, E.L., Marsman, D.S., Erasala, G.N., 2008. Safety evaluation of superabsorbent baby diapers. Regul. Toxicol. Pharmacol. 53, 81–89.

Lee, W.F., Chen, Y.C., 2005. Effect of intercalated reactive mica on water absorbency for poly(sodium acrylate) composite superabsorbents. Eur. Polym. J. 41, 1605–1612.

Li, A., Wang, A.Q., Chen, J.M., 2004. Studies on poly(acrylic acid)/attapulgite superabsorbent composite. I. Synthesis and characterization. J. Appl. Polym. Sci. 92, 1596–1603.

Lin, J.M., Wu, J.H., Yang, Z.F., Pu, M.L., 2001. Synthesis and properties of poly(acrylic acid)/mica superabsorbent nanocomposite. Macromol. Rapid. Commun. 22, 422–424.

Liu, P., 2007. Polymer modified clay minerals: a review. Appl. Clay Sci. 38, 64–76.

Liu, P.S., Li, L., Zhou, N.L., Zhang, J., Wei, S.H., Shen, J., 2007. Waste polystyrene foam-*graft*-acrylic acid/montmorillonite superabsorbent nanocomposite. J. Appl. Polym. Sci. 104, 2341–2349.

Luo, W., Zhang, W., Chen, P., Fang, Y., 2005. Synthesis and properties of starch grafted poly[acrylamide-*co*-(acrylic acid)]/montmorillonite nanosuperabsorbent via γ-ray irradiation technique. J. Appl. Polym. Sci. 96, 1341–1346.

Omidian, H., Hashemi, S.A., Sammes, P.G., Meldrum, I.G., 1998. A model for the swelling of superabsorbent polymers. Polymer 39, 6697–6704.

Omidian, H., Rocca, J.G., Park, K., 2005. Advances in superporous hydrogels. J. Control. Release 102, 3–12.

Pavlidou, S., Papaspyrides, C.D., 2008. A review on polymer-layered silicate nanocomposites. Prog. Polym. Sci. 33, 1119–1198.

Pourjavadi, A., Mahdavinia, G.R., 2006. Superabsorbency, pH-sensitivity and swelling kinetics of partially hydrolyzed chitosan-*g*-poly (acrylamide) hydrogels. Turk. J. Chem. 30, 595–608.

Pourjavadi, A., Barzegar, S., Mahdavinia, G.R., 2006. MBA-crosslinked Na–Alg/CMC as a smart full-polysaccharide superabsorbent hydrogels. Carbohydr. Polym. 66, 386–395.

Puoci, F., Iemma, F., Spizzirri, U.G., Cirillo, G., Curcio, M., Picci, N., 2008. Polymer in agriculture: a review. Am. J. Agric. Biol. Sci. 3, 299–314.

Ramazani-Harandi, M.J., Zohuriaan-Mehr, M.J., Yousefi, A.A., Ershad-Langroudi, A., Kabiri, K., 2006. Rheological determination of the swollen gel strength of superabsorbent polymer hydrogels. Polym. Test. 25, 470–474.

Ray, S.S., Okamoto, M., 2003. Polymer/layered silicate nanocomposites: a review from preparation to processing. Prog. Polym. Sci. 28, 1539–1641.

Ray, S.S., Bousmina, M., 2005. Biodegradable polymers and their layered silicate nanocomposites: in greening the 21st century materials world. Prog. Mater. Sci. 50, 962–1079.

Sadeghi, M., Hosseinzadeh, H.J., 2008. Synthesis of starch-poly(sodium acrylate-*co*-acrylamide) superabsorbent hydrogel with salt and pH-responsiveness properties as a drug delivery system. J. Bioact. Compat. Pol. 23, 381–404.

Wang, L., Zhang, J.P., Wang, A.Q., 2008. Removal of methylene blue from aqueous solution using chitosan-*g*-poly(acrylic acid)/montmorillonite superadsorbent nanocomposite. Colloid Surf. A 322, 47–53.

Wu, J.H., Wei, Y.L., Lin, J.M., Lin, S.B., 2003. Study on starch-*graft*-acrylamide/mineral powder superabsorbent composite. Polymer 44, 6513–6520.

Zheng, Y.A., Li, P., Zhang, J.P., Wang, A.Q., 2007. Study on superabsorbent composite XVI. Synthesis, characterization and swelling behaviors of poly(sodium acrylate)/vermiculite superabsorbent composites. Eur. Polym. J. 43, 1691–1698.

Zhu, R.L., Zhu, L.Z., Zhu, J.X., Xu, L.H., 2008. Structure of cetyl trimethylammonium intercalated hydrobiotite. Appl. Clay Sci. 42, 224–231.